ANALYSIS OF THE RELATIONSHIP BETWEEN THE Dst INDEX AND THE HELIOSPHERE PARAMETERS DURING OF CME- AND CIR-STORMS DEVELOPMENT

© 2025 N. A. Kurazhkovskaya*, B. I. Klain, O. D. Zotov***, A. Yu. Kurazhkovskii******

Borok Geophysical Observatory, Branch of the Schmidt Institute of Physics of the Earth, RAS (GO Borok IPE RAS), Borok, Yaroslavl oblast, Russia

**e-mail: knady@borok.yar.ru*

***e-mail: klain@*borok.yar.ru

****e-mail: ozotov@inbox.ru*

*****e-mail: ksasha@*borok.yar.ru

Received February 03, 2025

Revised March 10, 2025

Accepted May 22, 2025

Abstract. The analysis of the features of the average statistical dependence of the *Dst* index on the heliospheric parameters during the development of storms initiated by solar coronal mass ejections (CME-storms) and corotating interaction regions (CIR-storms) is carried out. It is found that the dynamics of the *Dst* index and the β-parameter (equal to the ratio of the thermal pressure to the magnetic pressure) during the development of storms caused by CME and CIR flows are qualitatively similar. In the main phase of CME- and CIR-storms, the average statistical value of the parameter $\beta < 1$ and $\beta > 1$, respectively. This is reflects different plasma turbulence in solar wind flows. It is shown that in the interval of CME- and CIR-storm development, the trajectory of *Dst* change depending on the heliosphere parameters in the main phase of storms does not coincide with its trajectory in the recovery phase. This is a typical feature of the hysteresis phenomenon. The hysteresis effect between the *Dst* index and the key parameters of the solar wind and interplanetary magnetic field (IMF) is observed during the development of both types of storms, indicating a nonlinear nature of the relationship between *Dst* and heliospheric parameters. The shape and size of the hysteresis loops vary depending on the analyzed parameters. The hysteresis loops for CIR-storms are smaller in area than the hysteresis loops for CME-storms. It was found that in the period preceding the occurrence of CME- and CIR-storms, the solar wind flows have a closed configuration of the IMF intensity vector *B* in the ecliptic plane with different rotation directions.

Keywords: *Dst-index, geomagnetic storms, solar wind, heliospheric parameters, coronal mass ejections, corotating interaction regions, turbulence, hysteresis*

DOI: 10.31857/S00167940250507e8

1. INTRODUCTION

According to modern concepts, e.g., [Gonzalez et al., 2007; Ermolaev et al., 2009; Richardson and Cane, 2012; Sun et al., 2024], there are several large-scale types of solar wind flows (drivers) that initiate perturbations in the Earth's magnetosphere. The most geoeffective plasma flows leading to the development of geomagnetic storms are usually considered to be coronal mass *ejections* on the Sun (CME - *Coronal Mass Ejection*) and *corotating* interaction regions of high-speed solar wind plasma flows from coronal holes on the Sun and slow solar wind flows (CIR - Corotating *Interaction Regions*) [Borovsky and Denton, 2006; Tsurutani et al., 2006; Guo et al., 2009; Turner et al., 2009]. This is due to the fact that these solar wind streams are characterized by the presence of a long period of the southern direction of the vertical component ($Bz < 0$) of the interplanetary magnetic field (IMF). Storms whose excitation is associated with CME and CIR solar wind streams are sometimes referred to as CME storms and CIR storms, e.g., [Borovsky and Denton, 2006; Turner et al., 2009]. Hereafter, for brevity, we will also use this terminology.

As is known, CME- and CIR-storms have a number of distinctive features in addition to the different origin of the flows causing them. For example, in [Borovsky and Denton, 2006] a list of differences between CME- and CIR-storms is given, let us name some of them. Thus, the storms associated with CME-streams of solar wind are mainly observed at the maximum of solar activity, they are irregular and, as usual, begin with a sudden onset (SSC - *Storm Sudden Commencement*). Unlike CME-storms, CIR-storms are observed during the phase of solar activity decline, they are characterized by 27-day recurrence and gradual onset (SGC - *Storm Gradual Commencement*). Storms caused by coronal mass ejections are characterized by high intensity but relatively short duration, whereas storms initiated by CIR are smaller in intensity but much longer in duration [Turner et al., 2009]. There are also some differences in the dynamics of solar wind and IMF parameters during the evolution of geomagnetic storms associated with CME- and CIR-induced storms, e.g., [Gupta and Badruddin, 2009; Yermolaev et al., 2009; Yermolaev et al., 2010; Yermolaev et al., 2010; 2011; Yermolaev et al., 2015; Dremukhina et al., 2019]. In addition, CME- and CIR-storms have different effects on wave activity of ultralow-frequency oscillations of *the Pc5* range [Kozyreva and Kleimenova, 2010; Simms et al., 2010; Potapov, 2013].

Previously, we found that the dynamics of the *Dst index*, which is an indicator of geomagnetic storms, and the variation of the β-parameter of the solar wind (the β parameter is equal to the ratio of plasma pressure to magnetic pressure) practically repeat each other during the development of storms with sudden and gradual onset [Kurazhkovskaya et al., 2021]. This behavior of *Dst* and β is characteristic of both weak and moderate storms and storms of strong intensity. The analysis of the relationship between the Dst-index and β-parameter [Kurazhkovskaya et al., 2021] showed that the *Dst*(β) dependence during the development of storms with sudden and gradual onset has a nonlinear

character. The question of whether there is a similarity between the dynamics of the Dst-index and the β-parameter, and what is the nature of the relationship between the *Dst-index* and the β-parameter during the development of CME- and CIR-storms remains open.

In another study [Kurazhkovskaya and Kurazhkovsky, 2023], it was found that the trajectory of *Dst* changes depending on the β-parameter during the main phase of storms did not coincide with its trajectory during the recovery phase, which was a typical sign of the hysteresis phenomenon. Moreover, the signs of hysteresis between *Dst* and β were manifested over the time interval of storm development, both with sudden and gradual onset. It was further shown [Zotov et al., 2024; Kurazhkovskaya et al., 2025] that the average statistical dependence of *Dst* on the dynamic pressure of the solar wind (Pdyn), the *Bz-component of* the MMP, and other heliospheric parameters also forms hysteresis loops over the development interval of storms of different intensities with sudden and gradual onset. Whether the signs of hysteresis between the *Dst-index* and heliospheric parameters are manifested during the development of CME- and CIR-storms has not been investigated yet.

One of the characteristics of solar wind inhomogeneities leading to the development of storms is the configuration of the magnetic field in the flow. As is known, the most intense perturbations on the Earth's surface are associated with large-scale solar wind streams having a closed configuration of the interplanetary magnetic field, of the magnetic cloud (MC - *Magnetic Cloud*) type [Burlaga et al., 1981]. Magnetic clouds are characterized by a high value of the MMP strength, a low value of the plasma parameterβ , and a smooth rotation of the magnetic field vector. Similar patterns are characteristic not only for MC flows, but also for mixed flows, which are formed as a result of the interaction of two or more separate fast flows [Burlaga et al., 1987]. For example, coronal mass *ejections* (*ejecta*) containing MCs and interacting with a corotating flux can be classified as a mixed flux [Burlaga et al., 1987]. Preliminary studies [Kline et al., 2022] have shown that it is likely that the solar wind streams prior to the onset of CME and CIR storms, have a closed magnetic field configuration similar to magnetic clouds. Further investigation of the structure of the MMP on the time interval preceding the development of CME- and CIR-storms is of undoubted interest. In spite of the fact that many publications analyzed the results of the impact of CME- and CIR-flows on the geomagnetic field and related perturbations, some aspects of the regularities of CME- and CIR-storms were left out of consideration.

Before proceeding to the presentation of the results of this work, the following clarifications are necessary. In our previous works [Kurazhkovskaya et al., 2021; Kurazhkovskaya and Kurazhkovsky, 2023; Zotov et al., 2024; Kurazhkovskaya et al., 2025], we considered the selection of storms only by the type of their onset (sudden or gradual) and intensity (weak, moderate, or strong). This was due to the specifics of the geomagnetic storm catalog used by us and referenced in

these papers. This catalog did not take into account the type of drivers causing geomagnetic storms. According to some formal indications, perturbations with SSC and with SGC are considered to be caused by CME- and CIR-flows, respectively, e.g., [Taylor et al., 1994; Obridko et al., 2013]. However, there is not sufficient evidence to claim that all storms with sudden onset are associated only with CME- and storms with gradual onset with CIR-flows of the solar wind. In the catalog we used earlier, storms caused by other geoeffective solar wind structures could be included in the category of storms with sudden and gradual onset besides CME- and CIR-storms, respectively. At the same time, it is of interest to investigate the relationship of the *Dst-index* with the β parameter and other interplanetary parameters during the development of storms whose driver has been identified.

The aim of this work is to investigate the features of the mean relationship between the *Dst-index* and heliospheric parameters during the development of storms whose driver is the CME- and CIR-flows of the solar wind.

2. DATA USED

To continue the statistical study of the relationship between the Dst-index and the β parameter and other heliospheric parameters, we used the list of geomagnetic storms from [Turner et al., 2009]. This paper lists observations of 118 cases of CME storms and 91 cases of CIR storms identified for the period from 1995 to 2004. Hourly averaged data on solar wind parameters, MMP, and Dst-index from the OMNI database (https://spdf.gsfc.nasa.gov/pub/data/omni/low_res_omni/) were used for the same time interval.

In [Turner et al., 2009], moderate and strong storms with minimum values of $Dst_{min} \leq$ -50 nTL were considered, for which the type of solar wind currents causing them, namely CME- and CIR-flows of the solar wind, was determined. For each storm, the date and time of onset, duration, and intensity (minimum *Dst-index* value) are presented.

To identify common or different regularities in the behavior of the interplanetary medium parameters during the development of CME and CIR storms, the method of epoch superposition was used. The moment of the beginning of the storms indicated in [Turner et al., 2009] was chosen as the zero point. The authors [Turner et al., 2009] identified the beginning of storms by the first decrease of the *Dst-index* corrected for the dynamic solar wind pressure. The dynamics of all solar wind and MMP parameters were analyzed over a relatively long time interval from -72 hours to +168 hours from the onset of the storms. The following key solar wind and IMF parameters and their combinations were used from the OMNI database: velocity *V*, proton density *N*, dynamic pressure Pdyn, helium ion/proton concentration ratio *Na/Np*, proton temperature *T*, IMF intensity modulus *B*, *Bx*-, *By*-, *Bz*- components of the IMF, *Ey*-component of the interplanetary electric field

(*Ey* = -*VBz*), and solar wind parameter β. In the OMNI database, the parameter β is defined from the expression: $\beta = (\frac{4.16T}{10^5} + 5.34) \cdot \frac{Np}{B^2}$, where *T* is the temperature (K), *Np* is the proton density (cm^{-3}), and *B* is the magnetic field magnitude (nTl). All parameters were taken in the GSE system.

3. RESULTS OF THE STUDY

3.1 Dynamics of hourly averages of the solar wind, IMF and Dst-index parameters during the development of CME- and CIR-storms

In many publications, the method of superposition of epochs is usually used in the study of heliospheric conditions leading to the development of storms caused by different types of solar wind. Depending on the task at hand and the storms under consideration, the authors analyze a different set of parameters of the interplanetary medium. For example, in [Turner et al., 2009], the list of storms from which we use, the variations of only two heliospheric parameters - velocity *V* and *Bz-component of* the MMP - obtained by the method of superposition of epochs during the generation of CME- and CIR-storms are given for the analyzed storms. In order to compare the average conditions in the solar wind and MMP favorable for the development of CME- and CIR-storms, we consider a wider range of heliospheric parameters. Fig. 1 shows the variations of hourly average values of the key parameters of the heliosphere and geomagnetic activity during the development of CME- and CIR-storms. For convenience of comparison of the parameter dynamics, they are shown in pairs for CME- and CIR-storms. One can see that the dynamics of all parameters is practically similar during the development of CME- and CIR-storms. An increase of such parameters as *V*, *N*, Pdyn, *Na/Np*, *T*, *B*, and *Ey* is observed near the onset of geomagnetic storms of both types and then their gradual decrease after the onset of the storms. During the development of CIR storms, in contrast to CME storms, velocity and temperature continue to increase after the onset of the storms. The decrease of these parameters begins in the recovery phase of CIR storms. The behavior of parameter β is fundamentally different from the dynamics of parameters *V*, *N*, Pdyn, *Na/Np*, *T*, *B*, and *Ey* during the development of CME- and CIR-storms. In contrast to the above parameters, which gradually increase before the onset of both types of storms, the β parameter, on the contrary, decreases. By the time the minimum value of the *Dst*-index is reached, the value of the parameter $\beta \sim 1$ for CIR-storms and $\beta < 1$ for CME-storms. Then β returns to background values over a long time interval. Before the onset of both CME-storms and CIR-storms, the *Bz* component of the MMP changes its direction from north to south.

Fig. 1.

Table 1.

At the external similarity of the dynamics of most parameters during CME- and CIR-storms, there are differences in the maximum or minimum values of heliospheric parameters for the two types of storms. Table 1 shows the mean peak values and standard deviations of the solar wind and MMP parameters corresponding to CME- and CIR-storms. It can be seen that the maximum values of Pdyn, *Na/Np*, *B*, and *Ey* are larger for CME-storms than for CIR-storms, while *N*, *V*, and *T* are conversely smaller. During CME-storms, the *Bz*-component of MMP and *Dst*-index take lower negative values compared to CIR-storms. Thus, the peak values of the main solar wind and MMP plasma parameters differ significantly during storms caused by different interplanetary drivers. These differences in the behavior of solar wind and MMP parameters during the evolution of CME- and CIR-storms have been pointed out by many researchers. Table 1 shows that the standard deviations for many solar wind and IMF parameters are comparable to the mean values or even exceed them. This is due to the large scatter of the parameters, especially in the generation of strong storms regardless of the type of interplanetary source. Such behavior of the standard deviation was previously discussed in [Ermolaev et al., 2010]. Nevertheless, estimates of the accuracy of the obtained mean values of the *Dst-index* and all interplanetary parameters showed that they do not exceed the limits of the confidence intervals with a probability of 0.95.

To answer the question whether there is a similarity between the dynamics of the Dst-index and the β parameter during the development of storms caused by CME- and CIR-flows of the solar wind, we consider the variation of these parameters together. Fig. 2 shows the average dynamics of *Dst* and *β* obtained by the epoch superposition method for CME- and CIR-storms over the interval from -48 to +72 hours relative to the storm onset. To exclude small fluctuations, the *Dst* and β data accumulated by the epoch superposition method were pre-smoothed by a moving average of 15 points. Figure 2 shows a qualitative coincidence of the dynamics of the β parameter with the behavior of the *Dst-index* during the development of storms initiated by CME- and CIR-flows. In the main phase of the storm, the β parameter gradually decreases in value (as well as *Dst*) and in the recovery phase it returns to the values before the onset of the storm. In the temporal neighborhood of the *Dst-index* minimum, the β parameter becomes close to 1 in magnitude. Thus, during the development of CME- and CIR-storms when *Dst* reaches its minimum values, the value of the β parameter is $\beta = 0.64$ and $\beta = 1.12$, respectively. Comparison of the behavior of *Dst* and β showed that the duration of the recovery phase of both CME- and CIR-storms follows the typical return time of the β parameter to background values. Previously, a similar pattern was found for storms with sudden and gradual onset in [Kurazhkovskaya et al., 2021]. The effect of the similarity of the mean dynamics of *Dst* and β-parameter is one of the features of the evolution of CME- and CIR-storms.

Fig. 2.

3.2 Hysteresis effect between the Dst-index and heliospheric parameters over the development interval of storms associated with CME- and CIR-flows of the solar wind

Next, we study the regularities of the relationship between the *Dst-index* and the solar wind and IMF parameters over the development interval of CME- and CIR-storms, the dynamics of which is shown in Fig. 1. First of all, we note that the durations of both CME-storms and CIR-storms from [Turner et al., 2009] varied widely. For example, the minimum and maximum durations of CME-storms were 15 h and 115 h, respectively, while CIR-storms were 12 h and 198 h, respectively. The mean duration of CME- and CIR-storms was 51 h and 69 h, respectively. Since we are analyzing the average dependencies between *Dst* and heliospheric parameters, we will use the accumulated hourly average data of *Dst* and heliospheric parameters at the time interval of 51 h and 69 h relative to the onset (zero point) of CME- and CIR-storms, respectively, by the epoch overlap method. The pre-accumulated parameter data were smoothed by a moving average of 15 points.

In the course of the study, it was found that the trajectory of *Dst* changes depending on the heliospheric parameters during the main phase of CME- and CIR-storms does not coincide with its trajectory during the recovery phase, which is a typical sign of the hysteresis phenomenon. Moreover, the *Dst* index forms a loop-like dependence with all analyzed parameters both during the development of CME- and CIR-storms. In Fig. 3 shows the dependences of *Dst*(*B*), *Dst*(*Bz*), *Dst*(Ey), *Dst*(*V*), *Dst*(*N*), *Dst*(*T)*, *Dst*(Pdyn), *Dst*(*Na/Np*), and *Dst*(β) on the development interval of CME- and CIR-storms. The curves of *Dst* dependence on heliospheric parameters for CME-storms are indicated by black circles, and for CIR-storms by gray circles. The beginning of the storm development process is shown with an asterisk. For convenience of comparison, all obtained dependences are presented in pairs for CME- and CIR-storms. The loop-shaped dependences between *Dst* and the analyzed parameters indicate the nonlinear nature of their relationship during the development of CME- and CIR-storms.

Fig. 3.

One of the conditions for the appearance of hysteresis loops is the phase shift between the analyzed parameters. The width of hysteresis loops in this case is proportional to the phase shift (time delay) between the *Dst-index* and heliospheric parameters. The larger the time delay, the wider the loop. Thus, *Dst* forms relatively wide loops with the parameters *B*, *Bz*, Ey, and *P*dyn and narrow loops with *V* andβ for both types of storms. In addition to width, the qualitative characteristics of hysteresis loops are usually their shape, area, and direction of rotation. As can be seen from the obtained diagrams (Fig. 3), the shape and size of hysteresis loops vary depending on the analyzed parameter. In most cases, the shape of hysteresis loops for CME- and CIR-storms is similar in many respects. At the same time, there are differences in the area of hysteresis loops

between *Dst* and interplanetary parameters during the development of CME- and CIR-storms. Thus, the hysteresis loops for CIR storms are smaller in area than the hysteresis loops for CME storms. The effect of *Dst*-index hysteresis has a regular character, practically with all heliospheric parameters. But, sometimes there is a complex configuration of the hysteresis loop, for example, in the *Dst*(β) dependence there is an intersection of the *Dst* trajectories in the main and recovery phases of storms.

The direction of rotation in the hysteresis loops characterizes the delay in the change of one parameter relative to another, thus reflecting the delay in the perturbation of the magnetosphere relative to the changing interplanetary conditions during the development of storms. For example, in the hysteresis loops formed by *Dst* с *B*, Ey, *N*, *T*, and *P*dyn, the direction of rotation is clockwise and with *Bz* counterclockwise during both CME- and CIR-storms. However, as a function of *Dst* versus *V*, *Na/Np* andβ , the direction of rotation in the hysteresis loops is different for CME- and CIR-storms. For CME-storms, the hysteresis loops of *Dst* с *V* andβ have clockwise rotation direction, while for CIR-storms, they have counterclockwise rotation direction. Also, different rotation direction is observed in the loops formed by *Dst* с *Na/Np* (in case of CME-storms - counterclockwise and CIR-storms - clockwise). The observed hysteresis effect between *Dst* and heliospheric parameters over the development interval of CME- and CIR-storms is also one of the features of these storm types.

3.3 Configuration of the mmp intensity vector in the solar wind streams preceding the development of CME- and CIR-storms

As noted above, large-scale solar wind streams with a closed configuration are the source of the most intense geomagnetic storms. Let us consider the configuration of IMFs in the solar wind streams before CME- and CIR-storms. Hodographs of the magnetic field vector in projection on the ecliptic plane can characterize the configuration of the IMF [Burlaga et al, 1981]. For this purpose, using the accumulated hourly average data of the *Bx*- and *By*-components of the MMP, we constructed the average statistical projections of the MMP *B* vector hodographs onto the XY plane of the solar-ecliptic coordinate system 48 hours before the onset of CME- and CIR-storms. The accumulated data of the *Bx*- and By-components of the MMP were pre-smoothed by a moving average of 19 points. The resulting hodographs for the CME- and CIR-storms are shown in Fig. 4. It can be seen that the MMP intensity vector *B* rotates relatively smoothly, forming an arc that is almost closed in the ecliptic plane. Such a trend in the behavior of *B* before the onset of storms is characteristic of both flows whose source is coronal mass ejections and corotating interaction regions. It is most likely that in the solar wind flow, the MMP force lines form a closed configuration. Based on the hodographs shown in Fig. 4, there is reason to believe that the fluxes

causing CME- and CIR-storms before reaching the magnetosphere have the form of closed formations in the ecliptic plane, similar to the configuration of IMFs in magnetic clouds [Burlaga et al., 1981]. Moreover, the mean statistical hodographs of the IMF vector *B* in the period preceding the development of CME- and CIR-storms have a different rotation direction. The average statistical hodograph of the MMP vector *B* before the development of CME- and CIR-storms has left rotation (counterclockwise) and right rotation (clockwise), respectively, in the ecliptic plane from the Sun-Earth line. In our opinion, the magnetic field structures with a closed configuration and different rotation direction of the *B* vector in the solar wind streams during the period preceding the development of both types of storms is their typical feature.

Fig. 4.

Let us compare the hodographs presented in Fig. 4 with the average statistical hodographs of the MMP vector *B* in the ecliptic plane before the development of storms with sudden and gradual onset. For brevity, storms with sudden and gradual onset will be conventionally referred to as SSC- and SGC-storms, respectively. The motivation for comparing the MMP vector *B* hodographs in the ecliptic plane prior to the development of CME-CIR and SSC-SGC storms is related to the fact that, according to authors such as [Taylor et al., 1994; Obridko et al., 2013], SSC storms are caused by coronal mass ejections, while SGC storms are associated with high-velocity fluxes from coronal holes, just like CME- and CIR-storms. Since the lists of storms that we took from [Turner et al., 2009] included only moderate and strong storms, we also used the lists of moderate and strong storms to construct the MMP hodographs before the onset of SSC- and SGC-storms. For this purpose, we used a sample of storms with minimum values of $Dst_{\min} \leq$ -50 nTL, which were previously analyzed in [Kurazhkovskaya et al., 2021; Kurazhkovskaya et al., 2025]. We had at our disposal the data of the **Bx-** and *By-* components of the MMP accumulated *by the* epoch superposition method *for* an interval of 48 h before the onset of 238 storms with sudden and 367 storms with gradual onset. Similarly, as in the construction of the hodographs in Fig. 4, the **Bx-** and By-component data were pre-smoothed with a moving average of 19 points. In Fig. 5 (similar to Fig. 4) shows the mean projections of the MMP *B* vector hodographs onto the XY plane of the solar-ecliptic coordinate system 48 hours before the onset of storms with sudden (SSC-storms) and gradual onset (SGC-storms). It can be seen that before the onset of SSC-storms, the MMP intensity vector *B* forms an arc close to a closed configuration. At the same time, the rotation direction of the MMP vector *B* is counterclockwise, just as in the case before the development of CME-storms. However, before the development of storms with gradual onset, such a tendency in the behavior of the intensity vector *B of* the MMP is not observed. The obtained hodograph of the *B* IMF behavior in the ecliptic plane before SGC-storms clearly indicates the absence of a closed configuration and a

mixed direction of rotation (first clockwise and then counterclockwise). Figures 4 and 5 clearly show the difference between the MMP *B* hodographs for CIR- and SGC-storms.

Fig. 5.

Thus, some regularities of CME- and CIR-storms are similar to the regularities of storms with sudden and gradual onset (e.g., the similarity of the dynamics of the *Dst*-index andβ - parameter during the development of storms, the nonlinear nature of the relationship between *Dst* and heliospheric parameters, the hysteresis effect, and others). At the same time, differences between CME-, CIR-storms and SSC-, SGC-storms are noted, in particular, in the behavior of the MMP intensity vector *B* in the solar wind flow preceding the onset of storms.

4. DISCUSSION

In this paper, we have investigated some aspects of geomagnetic storms caused by identified solar wind streams, namely CME- and CIR-streams. For this purpose, we used two independent lists of CME- and CIR-storms from [Turner et al., 2009]. The study showed that CME- and CIR-storms are characterized by the similarity of the mean dynamics of the *Dst*-index and β-parameter of the solar wind (Fig. 2), as well as for storms with sudden and gradual onset of different intensities [Kurazhkovskaya et al., 2021]. In this connection, there is reason to believe that the similarity of the variation of *Dst* and *β* has a universal character and does not depend on the type of storm onset (sudden or gradual), the storm strength (weak, moderate, or strong), and the type of driver (CME- or CIR-flows of the solar wind) that initiates the storm excitation.

In addition to the similarity of *Dst* and β dynamics during the development of CME- and CIR-storms, some features that distinguish these types of storms were found. Thus, during the development of CME- and CIR-storms, when *Dst* reaches its minimum values, the value of the β parameter isβ = 0.64 and β= 1.12, respectively. Near the minimum of *Dst index*, the parameter β takes values close to 1 during the development of both CME- and CIR-storms. The β parameter is a characteristic of the solar wind plasma turbulence [Borovsky and Funsten, 2003]. According to [Chernyshov et al., 2014], the level of turbulent fluctuations in the space plasma becomes maximum atβ ~ 1. Moreover, satellite observations have shown that a high degree of turbulence in the solar wind plasma is achieved at $0<\beta\leq1.3$ [Wang et al., 2018]. Thus, the excitation of CME- and CIR-storms is associated with solar wind streams whose plasma is highly turbulized. This supports the assumption [Kurazhkovskaya et al., 2021] that the turbulence of the solar wind plasma, characterized by the value of the parameterβ , can play a significant role in the process of geomagnetic storm evolution. Judging by the values of the parameter β = 0.64 and β = 1.12 at the maximum intensity of CME- and CIR-storms, respectively, the solar wind streams that are the drivers of these storms are characterized by different degrees of plasma turbulence.

Another feature of the investigated CME- and CIR-storms is the detection of a hysteresis effect in the dependences between the *Dst-index* and heliospheric parameters (Fig. 3). We investigated the relationship between *Dst* and nine key solar wind and IMF parameters and showed that the hysteresis effect actually occurs over the development interval of storms initiated by CME- and CIR-flows. From our point of view, the phenomenon of hysteresis between *Dst* and heliospheric parameters is also a universal property of geomagnetic storms. As shown by earlier studies [Kurazhkovskaya & Kurazhkovsky, 2023; Zotov et al., 2024; Kurazhkovskaya et al., 2025] and the results of this work, the hysteresis effect takes place regardless of the type of storm onset, intensity, and type of driver that cause them. Moreover, both statistical studies of the relationship between *Dst* and heliospheric parameters carried out by us and the analysis of individual magnetic storms [Danilova et al., 2024] indicate the existence of the hysteresis phenomenon between geomagnetic and interplanetary parameters on the scales of storm development.

The hysteresis effect indicates that the relationship between geomagnetic activity and interplanetary parameters during the development of CME- and CIR-storms, as well as during the development of storms with sudden and gradual onset, has a nonlinear character. During the evolution of CME- and CIR-storms, all investigated parameters change in a cyclic manner. As noted in Section 3.2, the observed signs of hysteresis in the dependences of *Dst* on heliospheric parameters are associated with phase shifts between these characteristics in the process of storm development. Practically all heliospheric parameters reach their maximum or minimum values not at the time of maximum storm intensity, but much earlier (Fig. 1). The obtained dependences of *Dst*(*B*), *Dst*(*Bz*), *Dst*(Ey), *Dst*(*V*), *Dst*(*N*), *Dst*(*T)*, *Dst*(Pdyn), *Dst*(*Na/Np*), and *Dst*(β) indicate different reactions of the magnetospheric perturbation to different solar wind and IMF parameters. This is manifested in the difference in the shape and size of the hysteresis loops. The areas of the hysteresis loops during the evolution of CME storms are much larger than for CIR storms, which reflects different phase shifts in time between *Dst* and heliospheric parameters during the evolution of these types of storms.

Taking into account the fact that the term "hysteresis" in the physics of solar-terrestrial relations was borrowed from the field of magnetism, we can draw an analogy between the processes in ferromagnetic materials under the influence of a magnetic field and the processes in the magnetosphere under the influence of the solar wind and MMP. Following this analogy, the size (width, area) of hysteresis loops is proportional to the energy required to return the magnetosphere to the unperturbed state. In other words, the area of the loops is proportional to the amount of energy dissipated in the magnetosphere during the hysteresis cycle as a result of the dissipation process. Based on the nonlinear nature of the relation between *Dst* and heliospheric parameters, we proposed a possible model to describe the interaction of the solar wind with the Earth's

magnetosphere during the development of storms [Kurazhkovskaya et al., 2025], which can be acceptable also for storms caused by CME- and CIR-flows.

One more peculiarity of CME- and CIR-storms should be paid attention to. Section 3.3 shows that the configuration of the MMP intensity vector in the solar wind flow in the ecliptic plane is closed before the onset of both types of storms, but with a different direction of rotation of the MMP vector *B* in the ecliptic plane. Magnetic clouds, whose source is coronal mass ejections, usually have a closed configuration. Magnetic clouds (as mentioned in the Introduction) are characterized by low values of the plasma parameter β (the magnetic pressure of the plasma is much higher than the thermal pressure). Indeed, during the development of CME storms, the average minimum value of $\beta = 0.64$, i.e. $\beta < 1$, is consistent with MC characteristics. A statistical study of the *B* MMP hodographs in the ecliptic plane has shown that not only magnetic clouds, but also other structures in the solar wind can have a closed field configuration. According to [Borovsky and Denton, 2006], the category of storms caused by CMEs includes storms induced by *ejecta* (or interplanetary ICMEs), CME *sheaths (*compression regions in front of ejecta/MC), and MCs. Given the variety of CME storm drivers and the magnitude ofβ -parameter, a closed configuration of the magnetic field before the onset of CME storms seems quite realistic, since ICME, *ejecta*, and MC have the same source on the Sun - solar flare and coronal mass ejections, which are closely related to each other. However, the fact that there is a closed configuration of the IMF before the onset of CIR storms, which have a minimum mean β = of 1.12, i.e. $\beta > 1$ (thermal pressure exceeds magnetic pressure), was unexpected.

The configuration of the fluxes before CME and CIR storms has counterclockwise rotation and clockwise rotation of the MMP vector *B*, respectively, in the ecliptic plane (Fig. 4). According to [Georgieva et al., 2005] solar wind structures with counterclockwise field rotation are more geoefficient than those with clockwise rotation. Consequently, the obtained MMP configurations confirm the known fact that CME fluxes are geoeffective than CIR fluxes [Borovsky and Denton, 2006].

The obtained discrepancy in the behavior of the MMP hodographs in the solar wind flow, presented in Figures 4 and 5 for CIR-storms and SGC-storms, can be attributed to many factors. For example, the magnetic storm catalog we used in [Kurazhkovskaya et al., 2021; Kurazhkovskaya et al., 2023] did not select the solar wind by flow type. On the other hand, the selection criteria for large-scale solar wind currents are relatively tentative. It is possible that the sources of CIR storms considered in [Turner et al., 2009] do not represent separate types of large-scale currents, but are mixed types of flows as discussed in [Burlaga et al., 1987]. From our point of view, the problem of analyzing the structure of solar wind streams preceding the development of storms requires further investigation.

Thus, as a result of this study, previously unknown differences in the fluxes causing CME- and CIR-storms have been revealed: 1) different degree of plasma turbulence of the solar wind (characterized by the value of the parameter β) when *Dst* reaches its minimum values, 2) difference in the size of hysteresis loops formed by the *Dst* index with the heliosphere parameters, 3) closed configuration of the magnetic field in the ecliptic plane with different direction of rotation of the MMP vector *B* during the period preceding the development of CME- and CIR-storms. In this regard, it can be assumed that among the factors determining the geoeffectiveness of the development-related fluxes may be the above-mentioned features. In conclusion, the results of this paper add to the list of differences between CME- and CIR-storms previously discussed in [Borovsky and Denton, 2006].

5. CONCLUSION

As a result of the epoch overlay analysis of 118 cases of CME storms and 91 cases of CIR storms identified for the period from 1995 to 2004, it was shown that the average statistical dynamics of key heliospheric parameters during the development of storms caused by coronal mass ejections on the Sun and corotating interaction regions are basically similar. One of the features of CME- and CIR-storms is the differences in the maximum or minimum values of heliospheric parameters. It was found that the qualitative behavior of the *Dst*-index and β parameter during the development of storms caused by CME- and CIR-flows is approximately similar to the dynamics of these parameters for storms with sudden and gradual onset. In the temporal neighborhood of the Dst-index minimum, the magnitude of the β parameter $\beta = 0.64$ and $\beta = 1.12$ for CME- and CIR-storms, respectively, reflects the different degree of plasma turbulence in the solar wind streams. A hysteresis effect in the dependences between *Dst* and heliospheric parameters during the development of both types of storms was found, which indicate the nonlinear nature of the relationship between *Dst* and interplanetary parameters. Differences in the size of hysteresis loops during storms initiated by CME- and CIR-flows of the solar wind are revealed. The hysteresis loops for CIR-storms are smaller in area than the hysteresis loops for CME-storms. It is found that during the period preceding the onset of CME- and CIR-storms, the solar wind streams have a closed configuration of the IMF in the ecliptic plane with a different rotation direction. CME-storms are characterized by left-handed rotation (counterclockwise), and CIR-storms by right-handed rotation (clockwise) of the IMF vector *B* in the ecliptic plane from the direction of the Sun-Earth line.

It is assumed that among the factors determining the geoeffectiveness of the flows associated with the development of CME- and CIR-storms may be: 1) different degree of turbulence of the solar wind plasma (characterized by the value of the parameterβ) when *Dst* reaches its minimum values, 2) difference in the size of hysteresis loops formed by the *Dst-index* with heliospheric

parameters, 3) closed configuration of the magnetic field in the ecliptic plane with different direction of rotation of the MMP vector *B* during the period preceding the development of CME- and CIR-storms.

ACKNOWLEDGEMENTS

The authors would like to thank the creators of the OMNI 2 database (*Goddard Space Flight Center*, NASA, USA) for the opportunity to use these data.

FUNDING

The work was carried out within the framework of the State Assignment of the Borok Geophysical Observatory of the Institute of Earth Physics of the Russian Academy of Sciences.

REFERENCES

1. *Danilova O.A., Ptitsyna N.G., Sdobnov V.E.* Hysteresis phenomena in the response of geomagnetic activity and cosmic ray parameters to variations in the interplanetary medium during a magnetic storm // Solar-terrestrial Physics. V. 10. No. 3. 2024. P. 70-78. https://doi.org/10.12737/szf-103202408

2. *Dremukhina L.A., Ermolaev Yu.I., Lodkina I.G.* Dynamics of interplanetary parameters and geomagnetic indices during periods of magnetic storms initiated by different types of solar wind // Geomagnetism and Aeronomy. 2019. V. 59. No. 6. P. 683-695. https://doi.org/10.1134/S0016794019060063

3. *Ermolaev Yu.I., Nikolaeva N.S., Lodkina I.G., Ermolaev M.Yu.* Catalog of large–scale solar wind phenomena for the period 1976-2000 // Space Research. V. 47. No. 2. P. 99-113. 2009.

4. *Ermolaev Yu.I., Lodkina I.G., Nikolaeva N.S., Ermolaev M.Yu.* Statistical study of the influence of interplanetary conditions on geomagnetic storms // Space Research. Vol. 48. No. 6. pp. 499-515. 2010.

5. *Ermolaev Yu.I., Lodkina I.G., Nikolaeva N.S., Ermolaev M.Yu.* Statistical study of the influence of interplanetary conditions on geomagnetic storms. 2. Variations of parameters // Space research. V. 49. No. 1. P. 24-37. 2011.

6. *Kline B.I., Zotov O.D., Kurazhkovskaya N.A.* Influence of the configuration of the interplanetary magnetic field (MMP) on the development of magnetic storms. The seventeenth Annual conference “Plasma Physics in the Solar System". Collection of abstracts. IKI RAS, Moscow, February 7-11, 2022, P. 146. 2022.

7. *Kozyreva O.V., Kleimenova N.G.* Variations of the ULF index of daytime geomagnetic pulsations during recurrent magnetic storms // Geomagnetism and Aeronomy. V. 50. No. 6. P. 799-809. 2010.

8. *Kurazhkovskaya N.A., Zotov O.D., Kline B.I.* The relationship between the development of geomagnetic storms and the β parameter of the solar wind // Solar-terrestrial Physics. V. 7. No. 4. P. 25-34. 2021. https://doi.org/10.12737/szf-74202104

9. *Kurazhkovskaya N.A., Kurazhkovsky A.Yu.* The effect of hysteresis between the geomagnetic activity indices (Ap, Dst) and the parameters of the interplanetary medium in the 21-24 cycles of solar activity // Solar-terrestrial Physics. V. 9. No. 3. P. 73-82. 2023. https://doi.org/10.12737/szf-93202308

10. *Kurazhkovskaya N.A., Kline B.I., Zotov O.D., Kurazhkovsky A.Yu.* Hysteresis cycles and invariance of the Dst index shape during the development of geomagnetic storms // Solar-terrestrial Physics. V. 11. No. 2. 2025. (in print).

11. *Obridko V.N., Kanonidi H.D., Mitrofanova T.A., Shelting B.D.* Solar activity and geomagnetic disturbances // Geomagnetism and aeronomy. V. 53. No. 2. P. 157-166. 2013. https://doi.org/10.7868/S0016794013010148

12. *Chernyshov A.A., Karelsky K.V., Petrosyan A.S.* Subgrid modeling for studying compressible magnetohydrodynamic turbulence of cosmic plasma // UFN. V. 184. № 5. P. 457-492. 2014. https://doi.org/10.3367/UFNr.0184.201405a.0457.

13. *Borovsky J.E., Funsten H.O*. Role of solar wind turbulence in the coupling of the solar wind to the Earth's magnetosphere // J. Geophys. Res. V. 108(A6). 1246–1258. 2003. https://doi.org/10.1029/2002JA009601

14. *Borovsky J.E., Denton M.H*. Differences between CME-driven storms and CIR-driven storms // J. Geophys. Res. V. 111. A07S08. 2006. https://doi.org/10.1029/2005JA011447

15. *Burlaga L.F., Sittier E.C., Mariani F., Schwenn R*. Magnetic loops behind an interplanetary shock: Voyager, Helios and IMP-8 observations // J. Geophys. Res. V. 86. Issue A8. P. 6673–6684. 1981. https://doi.org/10.1029/JA086iA08p06673

16. *Burlaga L.F., Behannon K.W., Klein L.W.* Compound streams, magnetic clouds, and major geomagnetic storms // J. Geophys. Res. V. 92. Issue A6. P. 5725–5734. 1987. https://doi.org/10.1029/JA092iA06p05725

17. *Georgieva K., Kirov B., Atanassov D., Boneva A*. Impact of magnetic clouds on the middle atmosphere and geomagnetic disturbances // J. Atmos. Sol. Terr. Phys. V. 67(1). P. 163–176. 2005. https://doi.org/10.1016/j.jastp.2004.07.025

18. *Gonzalez W.D., Echer E., Clua-Gonzalez A.L., Tsurutani B.T.* Interplanetary origin of intense geomagnetic storms (Dst < –100 nT) during solar cycle 23 // Geophys. Res. Lett. V. 34. L06101. 2007. https://doi.org/10.1029/2006GL028879

19. *Guo J., Feng X., Zhang J., Zuo P., Xiang C*. Statistical properties and geoefficiency of interplanetary coronal mass ejections and their heaths during intense geomagnetic storms // J. Geophys. Res. 2010. V. 115. A09107. https://doi.org/10.1029/2009JA015140

20. *Gupta V., Badruddin B*. Interplanetary structures and solar wind behaviour during major geomagnetic perturbations // Journal of Atmospheric and Solar-Terrestrial Physics. V. 71. P. 885–896. 2009. https://doi.org/10.1016/j.jastp.2009.02.004

21. *Potapov A.S*. ULF wave activity in high-speed streams of the solar wind: Impact on the magnetosphere // J. Geophys. Res. Space Physics. V. 118. P. 6465–6477. 2013. https://doi.org/10.1002/2013JA019119

22. *Richardson I.G., Cane H.V*. Solar wind drivers of geomagnetic storms during more than four solar cycles // J. Space Weather Space Clim. V. 2. A01. 2012. https://doi.org/10.1051/swsc/2012001

23. *Simms L.E., Pilipenko V.A., Engebretson M. J.* Determining the key drivers of magnetospheric Pc5 wave power // J. Geophys. Res. V. 115. A10241. 2010. https://doi.org/10.1029/2009JA015025

24. *Sun X., Zhima Z. Duan S., Hu Y., Lu C., Ran Z*. Statistical Analysis of the Correlation between Geomagnetic Storm Intensity and Solar Wind Parameters from 1996 to 2023 // Remote Sens. V. 16. 2952. 2024. https://doi.org/10.3390/rs16162952

25. *Taylor J.R., Lester M., Yeoman T.K*. A superposed epoch analysis of geomagnetic storms // Ann. Geophys. V. 12, iss. 7. P. 612–624. 1994. https://doi.org/10.1007/s00585-994-0612-4

26. *Tsurutani B.T., Gonzalez W.D., Gonzalez A.L.C., Guarnieri F. L., Gopalswamy N., Grande M., Kamide Y., Kasahara Y., Lu G., Mann I., McPherron R., Soraas F., Vasyliunas V*. Corotating solar wind streams and recurrent geomagnetic activity: A review // J. Geophys. Res. V. 111. A07S01. 2006. https://doi.org/10.1029/2005JA011273

27. *Turner N.E., Cramer W.D., Earles S.K., Emery B.A*. Geoefficiency and energy partitioning in CIR-driven and CME-driven storms // Journal of Atmospheric and Solar-Terrestrial Physics. V. 71. P. 1023–1031. 2009. https://doi.org/10.1016/j.jastp.2009.02.005

28. *Wang X., Tu C.-Y., He J.-S., Wang L.-H.* Ion-scale spectral break in the normal plasma beta range in the solar wind turbulence // J. Geophys. Res. Space Physics. V. 123. P. 68–75. 2018. https://doi.org/10.1002/2017JA024813

29. *Yermolaev Yu.I., Nikolaeva N.S., Lodkina I.G., Yermolaev M. Yu*. Specific interplanetary conditions for CIR-, Sheath-, and ICME-induced geomagnetic storms obtained by double superposed epoch analysis // Ann. Geophys., V. 28. P. 2177–2186. 2010. https://doi.org/10.5194/angeo-28-2177-2010

30. *Yermolaev Yu. I., Lodkina I. G., Nikolaeva N. S., Yermolaev M. Yu*. Dynamics of large-scale solar wind streams obtained by the double superposed epoch analysis // J. Geophys. Res. Space Physics. V. 120. P. 7094–7106. 2015. https://doi.org/10.1002/2015JA021274

31. *Zotov Oleg, Klain Boris, Kurazhkovskaya Nadezhda, Kurazhkovskii Alexander*. Hysteresis cycles and invariance of the *Dst* index form during geomagnetic storm development. 15th International Conference and School Problems of Geocosmos. Abstracts. St. Peterburg, Russia, April 22–26, 2024.

Table 1. Peak mean values and standard deviations of solar wind and IMF parameters, Dst-index, corresponding to CME- and CIR-storms

	CME-storms	CIR-storms
max *V*, km/s	533.29±156.31	546.63±98.53
max *N*, cm^{-3}	13.64±10.59	17.55±10.93
max Pdyn, nPa	7.74±8.75	5.29±3.26
max Na/Np*10^2	6.01±4.45	5.28±2.61
max T/10^4, K	18.76±18.64	23.89±13.71
max *B*, nTl	15.34±9.02	11.83±4.44
min *Bz*, nTl	-4.22±9.14	-2.02±5.14
max *Ey*, mV/m	2.29±4.82	1.33±2.17
min β	0.64±0.53	1.12±0.85
min *Dst*, nTl	-81.08±66.50	-45.42±21.34

FIGURE CAPTIONS

Fig. 1. Variation of hourly averages of the heliospheric parameters and geomagnetic activity during the development of CME- and CIR-storms. From top to bottom are given: (*a*) velocity *V*, proton density *N*, dynamic pressure Pdyn, helium ion to proton ratio *Na/Np*, temperature *T*; (*b*) MMP intensity modulus *B, Bz-component of the* MMP, *Ey-component of* the electric field,β solar wind parameter, *Dst-index*.

Fig. 2. Dynamics of the Dst-index (bold curves) and β-parameter (thin curves) during the development of CME- and CIR-storms.

Fig. 3. Hysteresis loops formed by geomagnetic activity (*Dst-index*) with heliospheric parameters: (*a*) - MMP intensity modulus *B*, (*b*) - Bz-component *of the* MMP, (*c*) - *Ey-component of* the electric field, (*d*) - velocity *V*, (*e*) - proton density *N*, (*f*) - proton temperature *T* of the solar wind plasma, (*g*) - the dynamic pressure Pdyn, (*h*) - the ratio of the concentration of helium ions and Na/Np protons, (*i*) - the β-parameter of the solar wind on the time interval of CME- and CIR-storm development. The beginning of the storm development process is indicated by an asterisk.

Fig. 4. Average projections of the MMP vector *B* hodographs onto the XY plane of the solar-ecliptic coordinate system 48 hours before the onset of CME- (black curve) and CIR- (gray curve) storms. The beginning of the rotation of the MMP vector *B* is indicated by the black circle.

Fig. 5. Average projections of MMP vector *B* traveltime curves on the XY plane of the solar-ecliptic coordinate system 48 hours before the onset of storms with sudden (SSC-storms) and gradual onset (SGC-storms), black and gray curves, respectively. The onset of the rotation of the MMP vector *B is* indicated by the black circle.

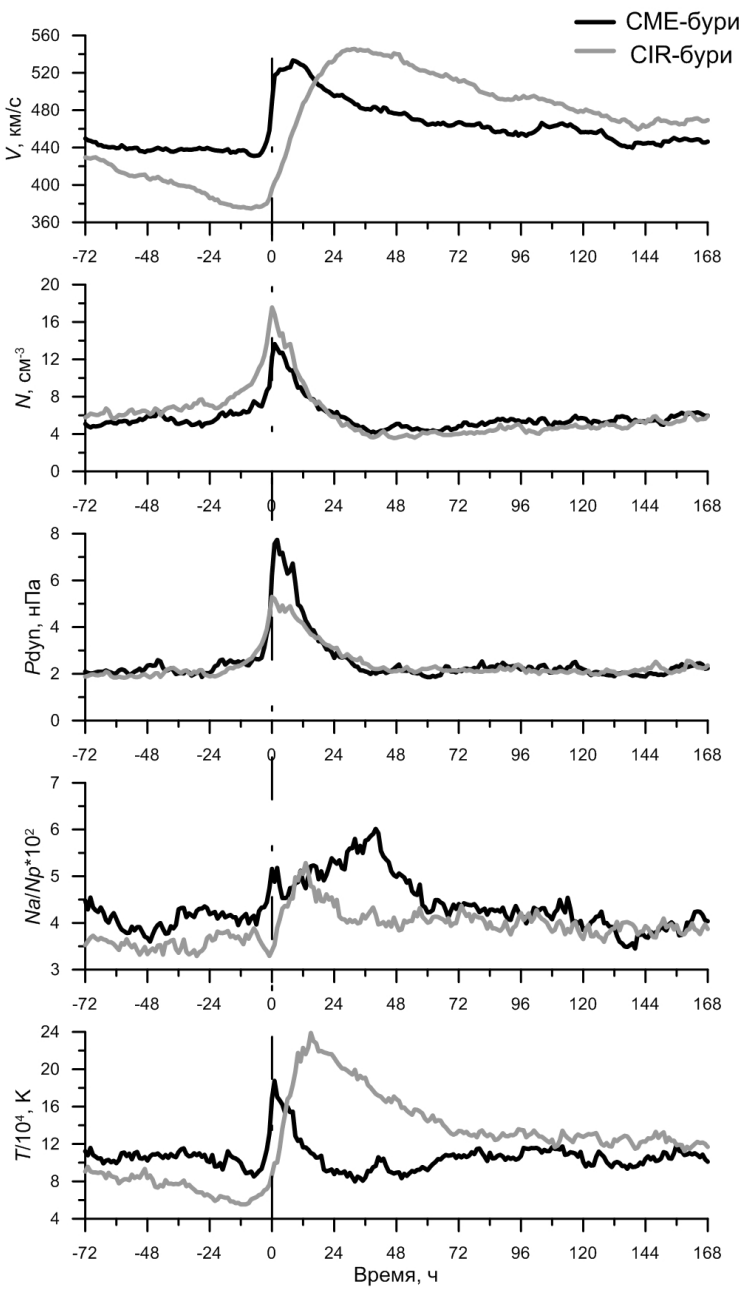

Fig. *1a*.

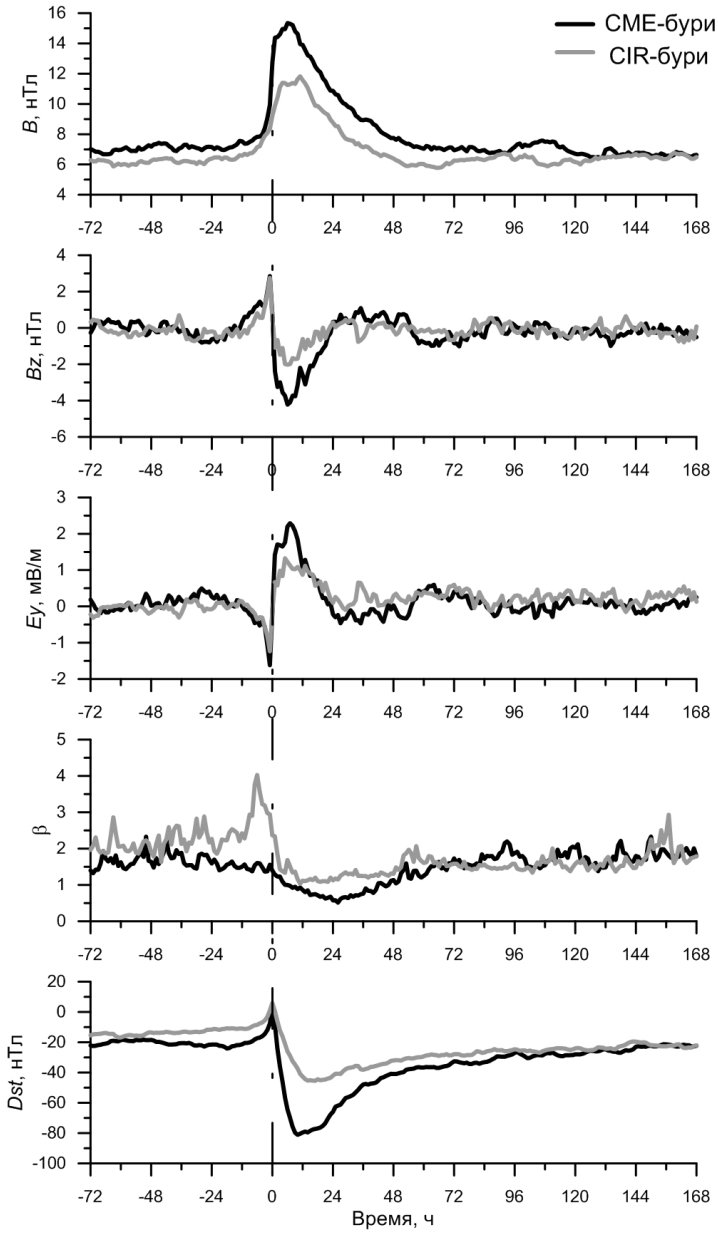

Fig. *1b*.

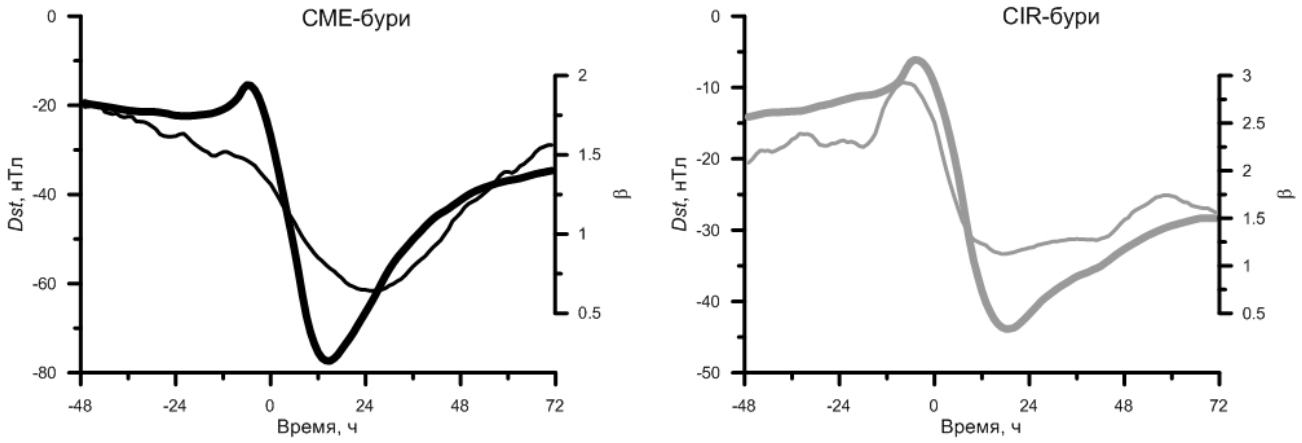
CME-бури
CIR-бури
Dst, нТл
β
Время, ч
0
-20
-40
-60
-80
-10
-30
-50
2
1.5
1
0.5
3
2.5
-48
-24
0
24
48
72

Fig. 2.

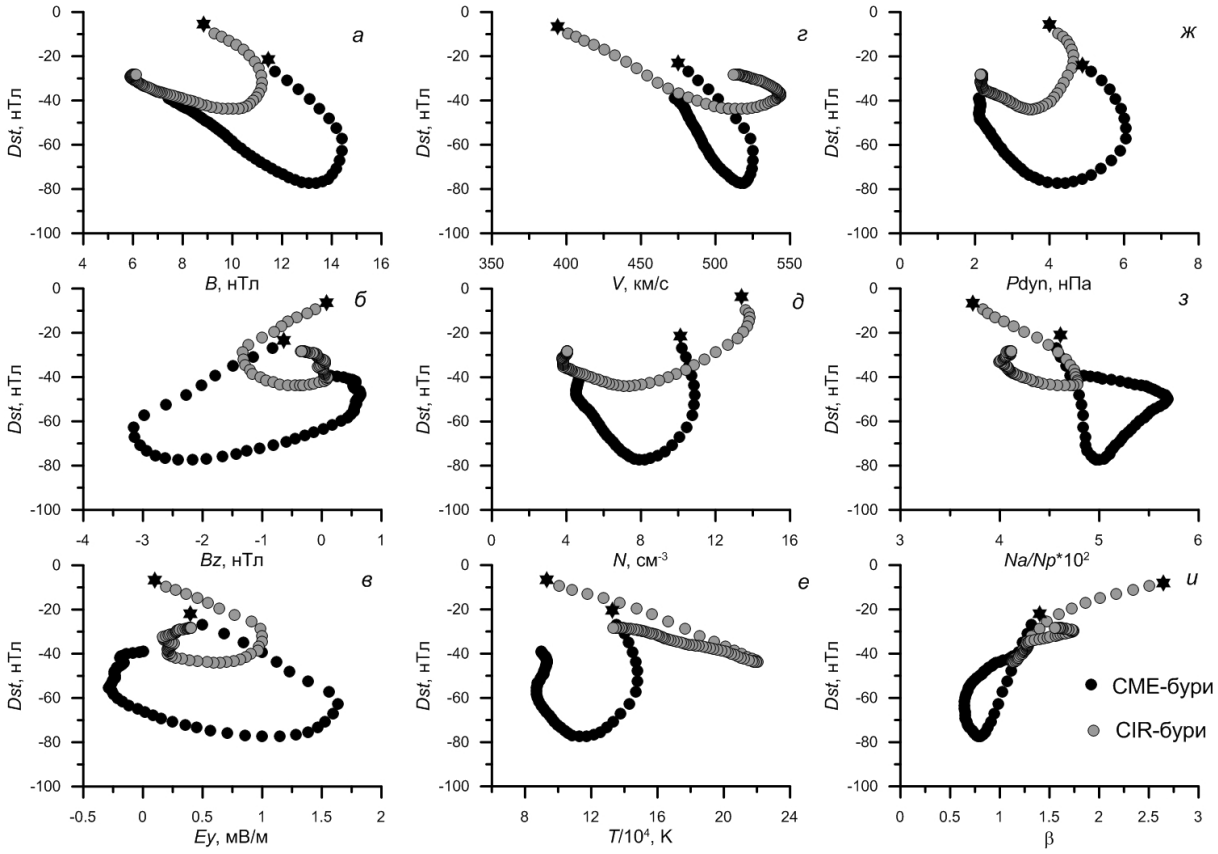
а
б
в
г
д
е
ж
з
и
Dst, нТл
B, нТл
Bz, нТл
Ey, мВ/м
V, км/с
N, см-3
T/10^4, K
Pdyn, нПа
Na/Np*10^2
β
CME-бури
CIR-бури

Fig. 3.

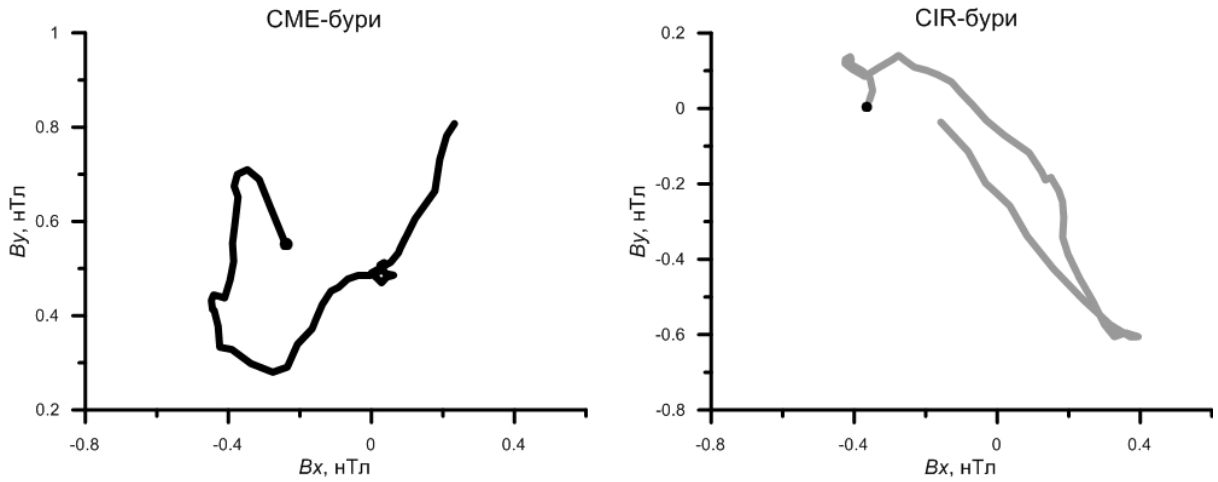
CME-бури
CIR-бури
By, нТл
Bx, нТл

Fig. 4.

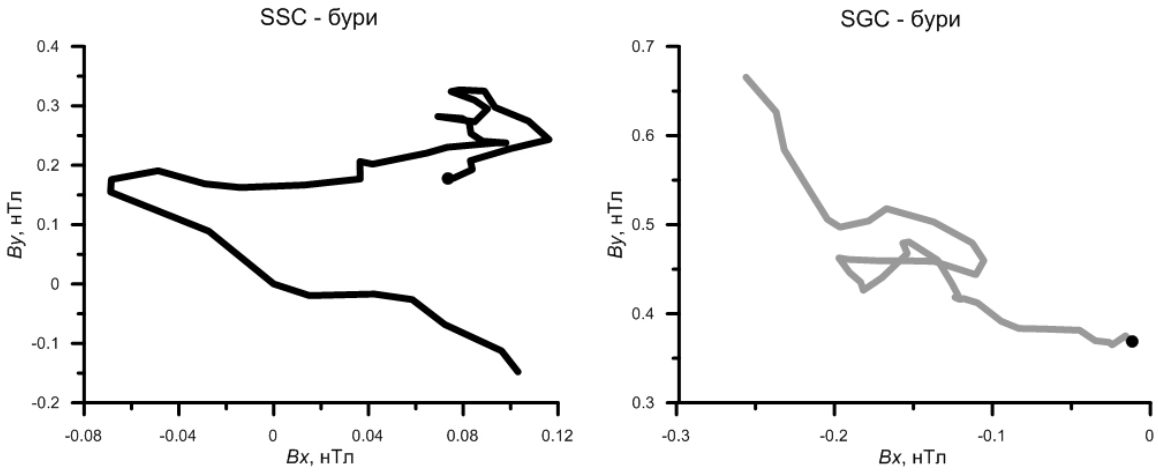
SSC - бури
SGC - бури
By, нТл
Bx, нТл
0.4
0.3
0.2
0.1
0
-0.1
-0.2
-0.08
-0.04
0
0.04
0.08
0.12
0.7
0.6
0.5
0.4
0.3
-0.3
-0.2
-0.1
0

Fig. 5.